

## Short-wave infrared ( $\lambda = 3 \mu\text{m}$ ) intersubband polaritons in the GaN/AlN system

T. Laurent, J.-M. Manceau, E. Monroy, C. B. Lim, S. Rennesson, F. Semond, F. H. Julien, and R. Colombelli

Citation: *Appl. Phys. Lett.* **110**, 131102 (2017); doi: 10.1063/1.4979084

View online: <http://dx.doi.org/10.1063/1.4979084>

View Table of Contents: <http://aip.scitation.org/toc/apl/110/13>

Published by the [American Institute of Physics](#)

---

---



Get the scoop on  
science funding & policy

Free sign-up  
for FYI emails

AIP American Institute of Physics

# Short-wave infrared ( $\lambda = 3 \mu\text{m}$ ) intersubband polaritons in the GaN/AlN system

T. Laurent,<sup>1</sup> J.-M. Manceau,<sup>1,a)</sup> E. Monroy,<sup>2</sup> C. B. Lim,<sup>2</sup> S. Rennesson,<sup>3</sup> F. Semond,<sup>3</sup> F. H. Julien,<sup>1</sup> and R. Colombelli<sup>1,b)</sup>

<sup>1</sup>Centre de Nanosciences et de Nanotechnologies, CNRS, Univ. Paris-Sud, Université Paris-Saclay, C2N-Orsay, 91405 Orsay Cedex, France

<sup>2</sup>Université Grenoble Alpes and CEA-INAC-PHELIQS, 17 av. des Martyrs, F-38000 Grenoble, France

<sup>3</sup>Université Côte d'Azur, CRHEA-CNRS, Rue Bernard Grégory, F-06560 Valbonne, France

(Received 27 January 2017; accepted 8 March 2017; published online 29 March 2017)

We demonstrate intersubband polaritons in the short-infrared wavelength range ( $\lambda < 3 \mu\text{m}$ ) relying on the GaN/AlN semiconductor system. The demonstration is given for an intersubband transition centered at  $\lambda = 3.07 \mu\text{m}$  ( $E = 403 \text{ meV}$ ). The polaritonic dispersion is measured at room temperature: a Rabi energy of  $53 \text{ meV}$  (i.e., a minimum splitting of  $106 \text{ meV}$ ), which represents  $13.1\%$  of the bare transition, is demonstrated. A metal-insulator-metal resonator architecture is employed, which proves to be efficient even at these short wavelengths. *Published by AIP Publishing.*  
[\[http://dx.doi.org/10.1063/1.4979084\]](http://dx.doi.org/10.1063/1.4979084)

Intersubband (ISB) polaritons stem from the strong light-matter coupling between an intersubband transition (more precisely: an ISB plasmon) and a microcavity photon mode. They were first observed at mid-IR frequencies,<sup>1</sup> with subsequent developments including ISB polariton LEDs,<sup>2</sup> polaritonic detectors/emitters,<sup>3,4</sup> ultra-fast switching,<sup>5,6</sup> and strong critical coupling.<sup>7</sup> The extension to the THz range of the spectrum was also realized, thanks to the use of metallic resonators.<sup>8</sup> The extension to the THz range was considered interesting because it provides access to the exotic regime of ultra-strong coupling.<sup>9–11</sup> The ultra-strong coupling regime was however demonstrated also in the mid-IR range of the spectrum.<sup>12,13</sup> In this regime, the anti-resonant terms of the hamiltonian (ab,  $a^\dagger b^\dagger$ , with  $a, a^\dagger$  the *photonic* operators, and  $b, b^\dagger$  the *electronic* ones) are not negligible. As a consequence, intriguing quantum electrodynamics phenomena have been predicted, such as Casimir radiation<sup>14</sup> and emission of non-classical light. To demonstrate these intriguing phenomena, it is however necessary to operate at shorter wavelengths, where detectors with high quantum efficiency exist. The extension of the ISB polaritons concept to shorter infrared wavelengths has been reported only once, in Ref. 15 at  $\lambda \sim 1.5 \mu\text{m}$  in the  $\text{Al}_{0.03}\text{Ga}_{0.97}\text{N}/\text{GaN}$  system. In Ref. 15, the idea was to employ meta-material cavities to attain extremely small interaction volumes. The electromagnetic field is indeed confined to deep sub-wavelength volumes; however, that architecture places the system only at the onset of the strong coupling regime.

Here, we demonstrate a GaN/AlN intersubband polariton system that operates at short infrared wavelengths ( $\lambda < 3 \mu\text{m}$ ), well into the strong-coupling regime and with the potential to access both shorter wavelengths and the ultra-strong coupling regime. We employ grating based-resonators that were originally developed for longer mid-IR wavelengths,<sup>16</sup> and we find that they still operate well at

these shorter wavelengths. Finally, we also demonstrate that operating in the strong-coupling regime permits to achieve narrower absorption resonances with respect to operation in the weak coupling regime. This is of interest, given the intrinsically relative large linewidth of ISB transitions in the GaN system.<sup>17</sup>

The sample is grown by  $\text{NH}_3$ -MBE in a Riber Compact 21 growth reactor. Growth is carried out on a FZ highly resistive Si(111) substrate. The active region and claddings are grown at  $800^\circ\text{C}$ . The  $150\text{-nm}$ -thick AlN buffer layer is nucleated at low temperature ( $600^\circ\text{C}$ ), and then, the temperature is rapidly ramped-up to  $1030^\circ\text{C}$  in order to improve the structural properties.<sup>18</sup> The structure consists of 18 repetitions of  $5\text{-nm}$ -thick n-doped GaN quantum wells (QWs) separated by  $2\text{-nm}$ -thick AlN barriers. This active region is sandwiched between thin  $\text{Al}_{0.29}\text{Ga}_{0.71}\text{N}$  claddings ( $30$  and  $82 \text{ nm}$ , respectively) to maintain a flat-band condition across the QW section.

Figure 1 shows the band structure in the conduction band for 3 periods of the structure. The first two electronic wavefunctions are confined by the triangular potential of the QW, induced by the strong internal spontaneous and piezoelectric field. The calculated bare transition energy is  $E_{12} = 382 \text{ meV}$ . However, the sample is heavily doped, the corresponding plasma energy is  $E_{\text{plasma}} = 285 \text{ meV}$ , and an

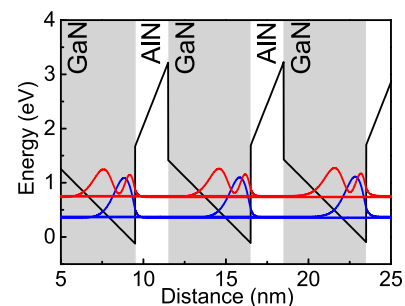


FIG. 1. Conduction band profile of the studied GaN/AlN heterostructure. The calculation has been performed with a Schrödinger-Poisson solver.

<sup>a)</sup>E-mail: jean-michel.manceau@u-psud.fr

<sup>b)</sup>E-mail: raffaele.colombelli@u-psud.fr

important depolarization shift is expected.<sup>19</sup> The sample is therefore expected to absorb at  $\hat{E} = \sqrt{E_{12}^2 + E_{plasma}^2} = 477$  meV.

We have characterized the room temperature ISB transition of the sample with two different techniques. First, we measured the transmission in a multi-pass waveguide configuration after polishing the facets at  $30^\circ$  angle, to avoid the total internal reflection at the silicon-GaN interface. A typical result is reported in Fig. 2(a). The absorption peak is slightly asymmetric, possibly a symptom of inhomogeneous broadening. It is centered at an energy  $E_{exp} = 403$  meV, with a full-width at half maximum (FWHM)  $\gamma_{12} = 146$  meV, that corresponds to 36% of the ISB energy.

The sample has been subsequently waferbonded to a GaAs host wafer using gold-gold thermo-compression techniques as detailed, for instance, in Ref. 20. At this point, the importance of performing the sample epitaxy on a silicon wafer becomes evident: the substrate must be selectively removed to expose the active region and obtain a semiconductor QW slab resting on a thick gold surface (inset of Fig. 2(b)). We employed a  $\text{XeF}_2$  gas-phase etching to perform this operation, since the process does not attack the GaN-based active region. The combination of high electronic doping and relatively low GaN index of refraction permits to measure the RT ISB absorption using a microscope equipped with a  $32\times$  Cassegrain objective and connected to a Fourier-transform infrared (FTIR) spectrometer. The measurement geometry is sketched in the inset of Fig. 2(b), while the figure reports the result of a typical measurement. The absorption peaks at the same energy as the multipass waveguide measurement. However, the FWHM is only 77 meV, corresponding to 19% of the ISB energy. The FTIR microscope performs the measurement on a  $50 \times 50 \mu\text{m}^2$  area, whereas the multi-pass approach probes a mm-sized area of the sample. This confirms the inhomogeneous origin of the broadening, which possibly stems from spatial non-uniformities across the sample surface.

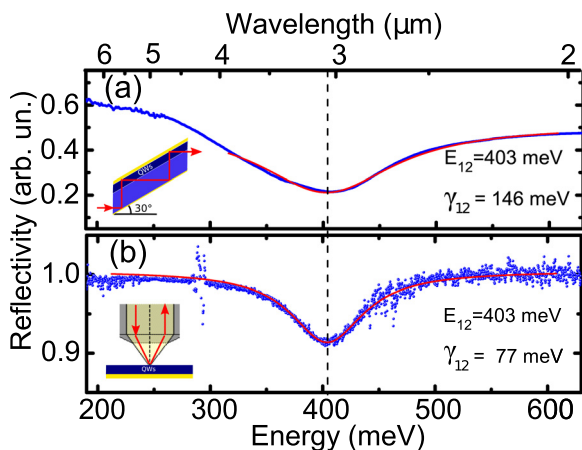


FIG. 2. (a) Sample transmission measured at room-temperature and in a multi-pass waveguide configuration with facets polished at  $30^\circ$ , as sketched in the inset. The measurement was performed using a FTIR spectrometer equipped with a beam-condenser. The source is a global lamp, and the detector is a room-temperature DTGS. (b) Sample reflectivity ( $R$ ) measured with an FTIR microscope. In this case the sample is waferbonded, via Au-Au thermo-compression, on a carrier substrate. Since there is no transmission, the measurement permits to directly gauge the absorption as  $1-R$ . In this case, the detector is liquid-nitrogen cooled Mercury Cadmium Telluride (MCT).

It is unusual to measure the ISB absorption using a FTIR microscope. In our case, it is possible, thanks to the sample high doping level and the relatively low refraction index of GaN. We can perform a quick estimate. Assuming that the back mirror is ideal, the measurement is equivalent to the transmission across a sample with twice the QW number (36 instead of 18). The Cassegrain objective focuses light onto the sample in an angular range between  $20^\circ$  and  $40^\circ$ . Assuming an average incidence angle of  $30^\circ$ , and the nominal doping density of  $5 \times 10^{19} \text{ cm}^{-3}$ , we can calculate  $\alpha_{2D}$ , the fraction of light absorbed by the 2D layer,<sup>21</sup> and hence estimate the sample absorption as 5.7%. This value is of the same order of magnitude as the experimental result (7.5%) and—given the crudeness of the approximation—is satisfactory and explains why this simple technique can be employed to measure the ISB transition energy, and also assess the degree of spatial inhomogeneity.

We have then implemented a top metallic grating on top of the wafer-bonded sample, as schematically shown in Fig. 3(a), a geometry that permits to easily perform reflectivity measurements<sup>22</sup> and extract the device photonic bandstructure. With a proper choice of the grating period, it is possible to superimpose the upper photonic branch at  $k_{||} = 0.42$  with the bare ISB transition energy, as the Rigorous Coupled Wave Analysis (RCWA) simulation in Fig. 3(b) shows. Strong light-matter coupling is then expected between the ISB plasmon and the photonic mode,<sup>16</sup> as presented in Fig. 3(c). The active region dielectric function is modeled using the Zaluźny–Nalewajko approach, as in Ref. 23.

The experimental reflectivity is measured using a FTIR spectrometer in combination with an angle resolved reflection unit. The results are presented in Fig. 4: the sample features a top metallic grating with a period  $\Lambda = 1.7 \mu\text{m}$  and a metal filling factor of 78%. It was realized by e-beam lithography followed by deposition of a Ti/Au metallic layer (5 nm/40 nm). The experimental band-structure in reflectivity is reported in Fig. 4(a): the upper polariton (UP) and lower polariton (LP) modes are clearly visible. The RCWA simulation reproduces the experimental data with a doping level of  $2.15 \times 10^{19} \text{ cm}^{-3}$ , lower than the nominal one. In turn, this permits to infer the value for  $E_{Rabi}$  as 53 meV. We also observe the presence of the 1st diffraction order that crosses the upper polariton branch and induces a reflectivity minimum at the crossing point. This system operates well in the short-wave IR region: at  $21^\circ$  incidence, the LP peaks at  $\lambda = 3.65 \mu\text{m}$  and the UP at  $\lambda = 2.7 \mu\text{m}$ . With the long-term goal of realizing an optically pumped ISB polariton laser<sup>24</sup> (the analog—for ISB transitions—of exciton-polariton lasers<sup>25,26</sup>) this GaN-based system is interesting since it permits to operate in a spectral region where pulsed laser sources with elevated peak power are available.

In this context, the question of the polariton linewidth naturally arises. Observing strong light-matter coupling with such levels of broadening is peculiar of ISB transition based systems, owing to the gigantic coupling constants that can be achieved by introducing elevated doping levels in the system, as it is the case here. We also observe a marked line narrowing of the polariton states with respect to the bare ISB transition. Figure 4(b) shows that the FWHM of the UP (LP) is  $\Gamma_{UP} = 10.6\%$  ( $\Gamma_{LP} = 13.5\%$ ) of the transition. This is way

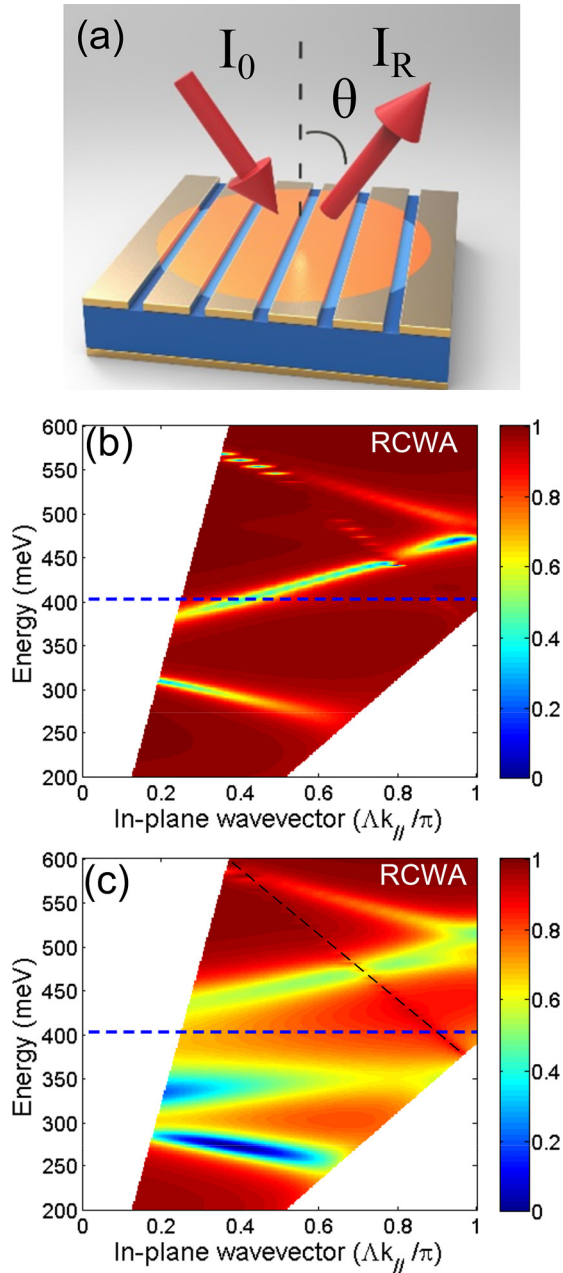


FIG. 3. (a) Schematics of the experimental geometry for angle-resolved reflectivity. (b) RCWA simulation of the reflectivity of the empty cavity. The reflectivity is plotted in the  $\omega$ - $k_{\parallel}$  space. (c) RCWA simulation of the reflectivity of the strongly coupled system (i.e., the polaritonic dispersion). The GaN heterostructure is modeled with the Zalusny-Nalewajko approximation,<sup>23</sup> using a doping level of  $2.15 \times 10^{19} \text{ cm}^{-3}$ , lower than the nominal one.

less than the linewidth of the ISB transition ( $\Gamma_{\text{ISB}}$ ) in weak coupling, which was estimated as 36% from multi-pass measurements, and 19% from microscope measurements. If we assume the latter value, the line narrowing can be explained considering that the polariton linewidth is the weighted average of the cavity ( $\Gamma_{\text{cav}}$ ) and the material excitation broadening. These grating-based resonators exhibit a  $\Gamma_{\text{cav}} = 5\%$  from the THz up to the mid-IR range of the electromagnetic spectrum.<sup>16,22</sup> Under the hypothesis that  $\Gamma_{\text{cav}}$  is similar at  $\lambda = 3 \mu\text{m}$ , we estimate a polariton linewidth of  $\sim 12\%$  (at the anti-crossing point), in agreement with the experiment.

However, the surface of the sample that is probed with the reflectivity measurements is much larger than the

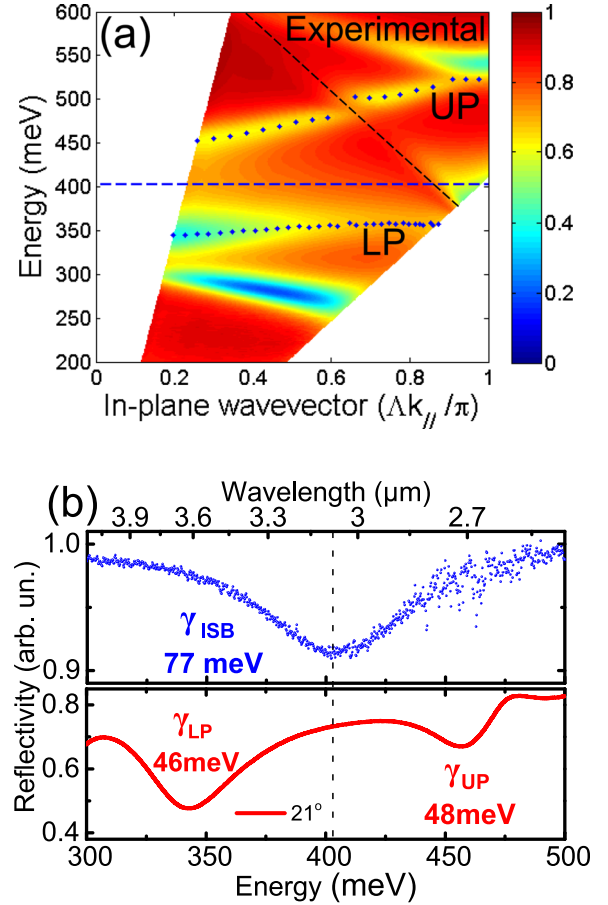


FIG. 4. (a) Experimental polaritonic dispersion measured at room-temperature via angle-resolved reflectivity measurements. Conversion from the  $\omega$ - $\theta$  space to the  $\omega$ - $k_{\parallel}$  space is readily obtained with the formula  $k_{\parallel} = (\omega/c)\sin\theta$ . The agreement between experiment and theory (Fig. 3(c)) is very good. (b) Comparison between the reflectivity of the strongly coupled system (measured at  $\theta = 21^\circ$ , lower panel) and the reflectivity of the weakly coupled system (no grating) measured with the FTIR microscope (upper panel). A clear line-narrowing is observed.

observation spot of the microscope; hence, the question arises why the broadening value of 36% is not at work here. In fact, it is not possible to invoke the resonator linewidth if we consider  $\Gamma_{\text{ISB}} = 36\%$ . Explaining this unexpected behavior is beyond the scope of this paper. We just highlight the experimental observation, and we suggest that a process analogous to the motional narrowing for exciton-polaritons could also be present for ISB polaritons too, as suggested, for instance, in Ref. 27, and also initially investigated in Refs. 12 and 28. In any case, the experimental finding is that operating in the strong coupling regime with the GaN system provides access to ISB-based transitions with much narrower linewidth than what can be achieved, with current technology, in this material system. This observation can be of interest in view of developing unipolar devices (detectors, for instance) operating at short-IR wavelengths.

We thank I. Roland for help with the  $\text{XeF}_2$  etching and P. Boucaud for useful discussions. This work was partly supported by the French RENATECH network. We acknowledge the financial support from the French National Research Agency via the GaNEX program (ANR-11-LABX-0014) and from ERC “GEM” grant (Grant Agreement No. 306661).



- <sup>1</sup>D. Dini, R. Köhler, A. Tredicucci, G. Biasiol, and L. Sorba, *Phys. Rev. Lett.* **90**, 116401 (2003).
- <sup>2</sup>L. Sapienza, A. Vasanelli, R. Colombelli, C. Ciuti, Y. Chassagneux, C. Manquest, U. Gennser, and C. Sirtori, *Phys. Rev. Lett.* **100**, 136806 (2008).
- <sup>3</sup>L. Sapienza, A. Vasanelli, C. Ciuti, C. Manquest, C. Sirtori, R. Colombelli, and U. Gennser, *Appl. Phys. Lett.* **90**, 201101 (2007).
- <sup>4</sup>M. Geiser, G. Scalari, F. Castellano, M. Beck, and J. Faist, *Appl. Phys. Lett.* **101**, 141118 (2012).
- <sup>5</sup>G. Günter, A. A. Anappara, J. Hees, A. Sell, G. Biasiol, L. Sorba, S. De Liberato, C. Ciuti, A. Tredicucci, A. Leitenstorfer, and R. Huber, *Nature* **458**, 178 (2009).
- <sup>6</sup>J. Lee, S. Jung, P.-Y. Chen, F. Lu, F. Demmerle, G. Boehm, M.-C. Amann, A. Alù, and M. A. Belkin, *Adv. Opt. Mater.* **2**, 1057 (2014).
- <sup>7</sup>S. Zanotto, F. P. Mezzapesa, F. Bianco, G. Biasiol, L. Baldacci, M. S. Vitiello, L. Sorba, R. Colombelli, and A. Tredicucci, *Nat. Phys.* **10**, 830 (2014).
- <sup>8</sup>Y. Todorov, A. M. Andrews, I. Sagnes, R. Colombelli, P. Klang, G. Strasser, and C. Sirtori, *Phys. Rev. Lett.* **102**, 186402 (2009).
- <sup>9</sup>C. Ciuti and I. Carusotto, *Phys. Rev. A* **74**, 33811 (2006).
- <sup>10</sup>G. Scalari, C. Maissen, D. Turčinková, D. Hagenmüller, S. De Liberato, C. Ciuti, C. Reichl, D. Schuh, W. Wegscheider, M. Beck, and J. Faist, *Science* **335**, 1323 (2012).
- <sup>11</sup>D. Dietze, A. M. Andrews, P. Klang, G. Strasser, K. Unterrainer, and J. Darmo, *Appl. Phys. Lett.* **103**, 201106 (2013).
- <sup>12</sup>E. Dupont, J. A. Gupta, and H. C. Liu, *Phys. Rev. B* **75**, 205325 (2007).
- <sup>13</sup>A. Delteil, A. Vasanelli, Y. Todorov, C. Feuillet Palma, M. Renaudat St-Jean, G. Beaudoin, I. Sagnes, and C. Sirtori, *Phys. Rev. Lett.* **109**, 246808 (2012).
- <sup>14</sup>C. Ciuti, G. Bastard, and I. Carusotto, *Phys. Rev. B* **72**, 115303 (2005).
- <sup>15</sup>A. Benz, S. Campione, M. W. Moseley, J. J. Wierer, A. A. Allerman, J. R. Wendt, and I. Brener, *ACS Photonics* **1**, 906 (2014).
- <sup>16</sup>J.-M. Manceau, S. Zanotto, T. Ongarello, L. Sorba, A. Tredicucci, G. Biasiol, and R. Colombelli, *Appl. Phys. Lett.* **105**, 81105 (2014).
- <sup>17</sup>H. Machhadani, P. Kandaswamy, S. Sakr, A. Vardi, A. Wirtmüller, L. Nevou, F. Guillot, G. Pozzovivo, M. Tchernycheva, A. Lupu, L. Vivien, P. Crozat, E. Warde, C. Bougerol, S. Schacham, G. Strasser, G. Bahir, E. Monroy, and F. H. Julien, *New J. Phys.* **11**, 125023 (2009).
- <sup>18</sup>F. Semon, *MRS Bull.* **40**, 412 (2015).
- <sup>19</sup>T. Ando, A. B. Fowler, and F. Stern, *Rev. Mod. Phys.* **54**, 437 (1982).
- <sup>20</sup>G. Xu, R. Colombelli, S. P. Khanna, A. Belarouci, X. Letartre, L. Li, E. H. Linfield, A. G. Davies, H. E. Beere, and D. A. Ritchie, *Nat. Commun.* **3**, 952 (2012).
- <sup>21</sup>E. R. Weber, R. K. Willardson, H. C. Liu, and F. Capasso, *Intersubband Transitions in Quantum Wells: Physics and Device Applications: Physics and Device Applications* (Academic Press, 1999).
- <sup>22</sup>J. M. Manceau, S. Zanotto, I. Sagnes, G. Beaudoin, and R. Colombelli, *Appl. Phys. Lett.* **103**, 091110 (2013).
- <sup>23</sup>M. Zalužný and C. Nalewajko, *Phys. Rev. B* **59**, 13043 (1999).
- <sup>24</sup>R. Colombelli and J.-M. Manceau, *Phys. Rev. X* **5**, 011031 (2015).
- <sup>25</sup>S. Christopoulos, G. B. H. von Högersthal, A. J. D. Grundy, P. G. Lagoudakis, A. V. Kavokin, J. J. Baumberg, G. Christmann, R. Butté, E. Feltn, J.-F. Carlin, and N. Grandjean, *Phys. Rev. Lett.* **98**, 126405 (2007).
- <sup>26</sup>D. Bajoni, *J. Phys. D: Appl. Phys.* **45**, 313001 (2012).
- <sup>27</sup>J. B. Khurgin and H. C. Liu, *Phys. Rev. B* **74**, 35317 (2006).
- <sup>28</sup>F. J. Murphy, A. O. Bak, M. Matthews, E. Dupont, H. Amrania, and C. C. Phillips, *Phys. Rev. B - Condens. Matter Mater. Phys.* **89**, 205319 (2014).